A parameterization of sulfuric acid-dimethylamine nucleation and its application in three-dimensional modeling

Yuyang Li[1, #], Jiewen Shen[1, 2, #], Bin Zhao[1, 2, *], Runlong Cai[3], Shuxiao Wang[1, 2], Yang Gao[4], Manish Shrivastava[5], Da Gao[1, 2], Jun Zheng[6], Markku Kulmala[2, 7, 8], Jingkun Jiang[1, *]

[1]State Key Joint Laboratory of Environment Simulation and Pollution Control, School of Environment, Tsinghua University, 100084 Beijing, China
[2]State Environmental Protection Key Laboratory of Sources and Control of Air Pollution Complex, Beijing, 100084, China
[3]Institute for Atmospheric and Earth System Research/Physics, Faculty of Science, University of Helsinki, 00014 Helsinki, Finland
[4]Key Laboratory of Marine Environment and Ecology, Ministry of Education, Ocean University of China, Qingdao 266100, China
[5]Pacific Northwest National Laboratory, Richland, Washington, USA
[6]School of Environmental Science and Engineering, Nanjing University of Information Science & Technology, Nanjing 210044, China
[7]Aerosol and Haze Laboratory, Beijing Advanced Innovation Center for Soft Matter Science and Engineering, Beijing University of Chemical Technology, 100029 Beijing, China
[8]Joint International Research Laboratory of Atmospheric and Earth System Sciences, School of Atmospheric Sciences, Nanjing University, Nanjing, China

[#] These authors contributed equally

[*] *Correspondence to*: Bin Zhao (bzhao@mail.tsinghua.edu.cn) and Jingkun Jiang (jiangjk@tsinghua.edu.cn)

Abstract. Sulfuric acid (SA) is a governing gaseous precursor for atmospheric new particle formation (NPF) in diverse environments, which is a major source of global ultrafine particles. In polluted urban atmosphere with high condensation sink (CS), the formation of stable SA-amine clusters, such as SA-DMA clusters, usually initializes intense NPF events. Coagulation scavenging and cluster evaporation are dominant sink processes of SA-amine clusters in urban atmosphere, yet they are not quantitatively included in the present parameterizations of SA-amine nucleation. We herein report a parameterization of SA-DMA nucleation based on cluster dynamic simulations and quantum chemistry calculations, with certain simplifications to greatly reduce the computational costs. Compared with previous SA-DMA nucleation parameterizations, this new parameterization would be able to reproduce the dependences of particle formation rates on temperature and CS. We then incorporated it in a three-dimensional chemical transport model to simulate the evolution of particle number size distributions. Simulation results show good consistency with the observations in the occurrence of NPF events and particle number size distributions in wintertime Beijing, showing a significant improvement compared to that using parameterization without coagulation scavenging. Quantitative analysis shows that SA-DMA nucleation contributes majorly to nucleation rates and aerosol population during the 3-D simulations in Beijing (>99% and >60%, respectively). These results broaden the understanding of NPF in urban atmospheres and stress the necessity of including the effects of coagulation scavenging and cluster stability in simulating SA-DMA nucleation in three-dimensional simulations. This would improve the performance in particle source apportionment and quantification of aerosol effects on air quality, human health, and climate.

1 Introduction

New particle formation (NPF) is the major source of atmospheric particles in terms of their number concentration, which regulates the Earth's radiative balance and affects the climate (Kulmala et al., 2004; Gordon et al., 2017; Merikanto et al., 2009). The transformation from gaseous precursors to stable clusters and particles via nucleation is the initial step of NPF, and new particle formation rate (J) is an essential parameter to characterize NPF intensity (Kulmala, 2003). Although nucleation processes would be suppressed by coagulation scavenging in urban atmospheres with high condensation sink (CS) (Cai and Jiang, 2017; Cai et al., 2017b), intense NPF events have been frequently observed (Wu et al., 2007; Xiao et al., 2015; Deng et al., 2020). Recently increasing evidence has been provided that those intense events are driven by the formation of stable SA-amine clusters (Cai et al., 2022; Jen et al., 2014b; Yin et al., 2021) with a speed close to the collision limit for SA molecules, thus deriving high nucleation rates in urban atmospheres (Cai et al., 2021d; Yao et al., 2018; Chen et al., 2012). Furthermore, other molecules, such as HNO_3 and NH_3, could enhance the SA-DMA nucleation under certain conditions (Liu et al., 2021; Glasoe et al., 2015; Wang et al., 2021). Although a few previous 3-D simulation studies have simulated NPF events in polluted urban atmospheres such as Beijing, they didn't take the SA-amine nucleation into account (Chen et al., 2019; Chen et al., 2021b).Thus, integrating SA-amine nucleation into three-dimensional (3-D) models would be essential in extending the understanding of NPF in polluted urban areas and quantifying its underlying impacts on the environment and climate. This requires a quantitative representation of particle formation rates through SA-amine nucleation for 3-D models.

Semi-empirical power-law functions are widely used in SA-relevant nucleation rate studies to fit the experimental data, which has been shown to reproduce the measured J in certain ambient observations or experimental conditions (Riccobono et al., 2014; Dunne et al., 2016; Bergman et al., 2015; Hanson et al., 2017; Semeniuk and Dastoor, 2018; Kurten et al., 2014; Kurten et al., 2018). For SA-amine nucleation, Bergman et al. (2015) and Dunne et al. (2016) have presented semi-empirical parameterizations of good consistencies with chamber and flow-tube experimental results (Almeida et al., 2013; Jen et al., 2014b; Glasoe et al., 2015). In real urban atmosphere, recent advances have shown that coagulation scavenging would greatly suppress concentrations of molecular clusters, and thus the nucleation rates (Cai and Jiang, 2017; Cai et al., 2021c; Cai et al., 2021d; Marten et al., 2022). It has also been addressed that the formation of the smallest SA-amine clusters, which is largely dependent on cluster stability, is the limiting step for SA-amine nucleation rates (Cai et al., 2022). However, the effects of coagulation scavenging and cluster stability would vary with the environmental factors, e.g., CS and temperature, while these effects have not been well represented in semi-empirical power-law functions derived from certain experimental systems or ambient environments. Cluster kinetic simulations coupled with quantum chemistry calculations (Mcgrath et al., 2012), which take into account the effects of both coagulation scavenging and cluster stability, have been widely applied in zero-dimensional or one-dimensional simulations of SA-NH_3 or SA-amine nucleation (Yang et al., 2021; Lu et al., 2020; Yao et al., 2018; Yu, 2006; Yu and Turco, 2001). Specifically, both cluster kinetic simulations and observations reveal that dimethylamine (DMA) is plausibly most efficient in stabilizing SA clusters and is regarded as the key amine species deriving high particle formation rates in urban atmosphere (Jen et al., 2014b; Cai et al., 2022; Yao et al., 2018; Chen et al., 2012). However, no method with good representations of coagulation scavenging and cluster stabilities has been reported to explicitly simulate the SA-DMA nucleation rates in 3-D chemical transport models.

A challenge in setting up a parameterization based on cluster kinetic simulations for 3-D chemical transport models is to reduce computational costs and yield explicit expressions. A plausible method to reduce computational costs is to omit the unstable clusters with high evaporation rates from the nucleation pathway. Accordingly, different nucleation schemes were presented to represent the dominant source or sink processes of SA-DMA clusters in specific chamber experiments or ambient environments (Lu et al., 2020; Cai et al., 2021d). For polluted urban atmospheres, a kinetic model with a key pathway of particle formation in SA-DMA nucleation was constructed, yielding good predictions of measured SA cluster concentrations and 1.4 nm particle formation rates ($J_{1.4}$) in urban Beijing (Cai et al., 2021d). Application of pseudo-steady-state assumptions

80 is also an alternative method for reducing computational costs and yielding explicit expressions. The NPF occurrence indicator
81 (*I*) based on the kinetic model with pseudo-steady-state assumptions has shown good consistency in qualitatively estimating
82 the NPF events in urban Beijing and Shanghai (Cai et al., 2021c). These results indicate the potential of deriving an explicit
83 parameterization of particle formation rates by applying pseudo-steady-state assumptions to the kinetic model, although further
84 quantitative analysis is still required to validate this parameterization.

85 In this study, we set up an SA-DMA nucleation parameterization, which is designed for application in 3-D chemical transport
86 models. The parameterization is based on the pseudo-steady-state particle formation rate in the kinetic model, with a full
87 representative of the effects of coagulation scavenging and cluster stability (Cai et al., 2021d). Generally, only four variables
88 (temperature T, CS, gaseous DMA concentrations [B], and concentrations of SA molecules or clusters containing one SA
89 molecule [SA_{tot}]) are used in the parameterization, with computational costs greatly reduced. We then implement the
90 parameterization in a 3-D chemical transport model and combine it with an integrated source-sink representation of DMA to
91 simulate the evolution of the particle number size distributions (PNSDs) in wintertime Beijing. The precursor concentrations,
92 PNSDs, NPF occurrence and $J_{1.4}$ show relatively good consistencies between simulations and observations. The simulations
93 show that the SA-DMA nucleation contributes >99% of the $J_{1.4}$ and >60% of the total particle number concentration in
94 wintertime Beijing, respectively. With this parameterization, 3-D chemical transport models could significantly improve the
95 simulation of NPF, especially in urban environments, and thus the effects of NPF on particulate matter pollution or climate.

96 2 Methods

97 2.1 Derivation of Parameterized Formation Rate in SA-DMA Nucleation

98 Limited by computational quantum chemistry calculation results, SA-DMA nucleation is commonly simulated in the range of
99 clusters containing not more than 4 SA or 4 DMA molecules (Olenius et al., 2013; Ortega et al., 2012). As unstable clusters
100 would evaporate with higher rates, the formation of larger clusters potentially follows the pathways of the most stable clusters.
101 In addition, as the SA-DMA clusters are increasingly stable along the main pathway of cluster formation, the clusters not
102 smaller than A_4B_4 (hereafter A_mB_n refers to clusters containing m SA and n DMA molecules) is assumed to not evaporate back
103 in these simulations. Although there are uncertainties in the pathways presented based on different quantum chemistry methods,
104 it is well accepted that the A_mB_m (m=1 to 4) and A_2B_1 clusters are relatively stable in the SA-DMA nucleation scheme (Olenius
105 et al., 2017; Olenius et al., 2013; Ortega et al., 2012; Myllys et al., 2019).

106 Under atmospheric conditions, the variation of temperature, CS and precursor concentrations would not bring large deviations
107 to the main pathway. Previous simulations under different [SA], [DMA], and temperature have showed shown that the main
108 pathway is similar under different conditions (Olenius et al., 2013). The effect of CS on nucleation pathway is dependent on
109 the relative relationship between the coagulation sink and the evaporation rate of a certain cluster. For most clusters out of the
110 specified pathway, the evaporation rates are much higher than the typical CS range in urban atmosphere (Ortega et al., 2012),
111 therefore they would not dominate the nucleation pathway no matter how high the CS is. Thus in this study, the variation of
112 the dominant pathway under different conditions would be ignored.

113 Accordingly, the parameterization in this study is derived from the nucleation pathway including A, B and other 5 SA-DMA
114 clusters (A_mB_m (m=1 to 4) and A_2B_1), consistent with a previous study (Cai et al., 2021d). The clusters except A_4B_4 are assumed
115 to be in pseudo-steady states, i.e. the sink due to evaporation, coagulation scavenging, and cluster collision is equal to the
116 source due to the collisions of molecules or smaller clusters. As the A_4B_4 clusters are estimated to be with an electrical mobility
117 diameter of approximately 1.4 nm, the pseudo-steady-state formation rate of A_4B_4 would be applied in the parameterization of
118 $J_{1.4}$ in this study.

2.1.1 Derivation of Collision Coefficients, Coagulation Sink, and Evaporation Rates

In the nucleation pathway discussed above, A, B, and 5 SA-DMA clusters are included. The collision coefficients between them ($\beta_{i\text{-}j}$) and the evaporation rate of A_1B_1 clusters (γ) would vary with T during the simulation. The coagulation sinks (CoagS$_i$) due to the coagulation scavenging of background aerosols are dependent on CS. The work discussed in this section is focused on simplification of the derivation of these parameters to be updated in each simulation time interval to reduce the computational costs.

As the involved clusters and molecules are in the free molecular regime (Knudsen number > 10), $\beta_{i\text{-}j}$ in SA-DMA nucleation processes can be calculated based on kinetic gas theory (Seinfeld and Pandis, 1998; Olenius et al., 2013; Ortega et al., 2012):

$$\beta_{i\text{-}j} = \left(\frac{3}{4\pi}\right)^{1/6}\left(\frac{1}{m_i}+\frac{1}{m_j}\right)^{1/2}\left(V_i^{1/3}+V_j^{1/3}\right)^2\left(6k_\text{b}T\right)^{1/2}E_{ij}, \tag{1}$$

where m (kg) and V (m^3) represent the molecular mass and molecular volume, respectively. The density of precursor molecules A and B was assumed to be 1830 and 680 kg m^{-3}, respectively. T (K) represents the temperature. k_b (J K^{-1}) is the Boltzmann constant. Subscripts i and j refer to the index of the clusters or molecules (1 to 7 refer to A, B, A_1B_1, A_2B_1, A_2B_2, A_3B_3, and A_4B_4, respectively, which are involved in the kinetic model). E_{ij} is a dimensionless enhancement factor of the collision rates from Van de Waals forces between i and j. In this study, E_{ij} is assumed to be 2.3 (Chan and Mozurkewich, 2001; Sceats, 1989), within the range of 2.3 to 2.7 predicted by Brownian coagulation models, and consistent with the value used in other cluster dynamics studies (Kurten et al., 2014; Lehtipalo et al., 2016; Stolzenburg et al., 2020).

Noting that m_i and V_i are almost independent of the atmospheric conditions and E_{ij} is assumed to be constant, we can normalize different values of $\beta_{i\text{-}j}$ into β, and the normalizing factor is shown in a look-up table (Table S1 in the supporting information (SI)) as $G(i,j)$:

$$\beta_{i\text{-}j} = \beta G(i, j), \tag{2}$$

where β represents the collision coefficients between two A_1B_1 clusters ($\beta_{3\text{-}3}$), and could be calculated as:

$$\beta = \beta_0\left(\frac{T}{T_0}\right)^{0.5}, \tag{3}$$

where β_0 is the value of β at the standard temperature T_0=298.15 K, constant as 1.126×10^{-15} m^3 s^{-1}.

Similarly, CoagS$_i$ could also be normalized to CS using fixed ratios. The size dependent coagulation sink (CoagS) is calculated with a power-law exponent of -1.7, within the typical range of atmospheric aerosols (Lehtinen et al., 2007):

$$CoagS_i = CS\left(\frac{V_i}{V_1}\right)^{-\frac{1.7}{3}}=H(i)CS, \tag{4}$$

where the dimensionless factors $H(i)$ are also recorded in Table S1 in the *SI*.

The evaporation rates of A_1B_1 could be derived based on collision-evaporation equilibrium (Ortega et al., 2012), closely relevant to the free energy barrier to form A_1B_1 clusters (Olenius et al., 2013; Ortega et al., 2012):

$$\gamma = \beta_{1\text{-}2}c_\text{ref}\exp\left(\frac{\Delta G}{k_BT}\right), \tag{5}$$

where c_ref is the number concentrations under standard conditions (2.46×10^{25} m^{-3}). ΔG is the formation free energies of A_1B_1. Thus if we take $T_0 = 298.15$ as a reference, γ could also be calculated as:

$$\gamma = \gamma_0\left(\frac{T}{T_0}\right)^{0.5}\exp\left(\frac{\Delta H}{k_\text{B}}\left(\frac{1}{T}-\frac{1}{T_0}\right)\right), \tag{6}$$

$$\gamma_0 = \gamma_0'\exp\left(\frac{\Delta G-\Delta G_0}{k_\text{B}T_0}\right), \tag{7}$$

where γ_0', with the value of 3.33 s^{-1}, is the evaporation rates of A_1B_1 at T_0 with $\Delta G=\Delta G_0$=-13.54 kcal mol^{-1}. ΔH is the formation enthalpies of A_1B_1. In previous studies, several sets of ΔH and ΔG at specific temperatures were reported based on different

155 quantum chemistry models (Myllys et al., 2019; Ortega et al., 2012; Ge et al., 2020a). Here we use ΔH = -24.82 kcal mol^{-1} and

156 ΔG = -13.54 kcal mol^{-1} according to the results in Myllys et al. (2019). If the values of ΔG need to be updated in future

157 application of this parameterization, the values of γ_0 should be updated as well based on Eq. 7. The sensitivity analysis of

158 different values of ΔH and ΔG are discussed in the Results section.

159 Generally, with $G(i,j)$ and $H(i)$ fixed into the parameterization formula, β_{i-j} and CoagS$_i$ could be normalized to β and CS.

160 Additionally, the values of γ and β could be real-time updated at any simulation timestep based on Eqs. 3 and 6.

2.1.2 Formula of the SA-DMA Nucleation Parameterization

162 Applying the pseudo-steady-state assumptions to the key pathway discussed above (Eqs. S1 to S9) and achieving real-time γ

163 (s^{-1}) and β (m^3 s^{-1}) (Eqs. 3 and 6), we could derive an explicit formula of the parameterized $J_{1.4}$ in this study (Eq. 8).

$$J_{1.4} = \frac{\beta\theta'[A_1B_1]^4}{2([A_1B_1]+0.39\frac{CS}{\beta})}\left(\frac{0.23\theta'}{[A_1B_1]+0.39\frac{CS}{\beta}}+\frac{1.00}{[A_1B_1]+0.31\frac{CS}{\beta}}\right), \tag{8}$$

165 The above intermediate parameters are calculated as below:

$$[A_1B_1] = \frac{0.96[B][SA_{tot}]}{0.96[B]+\frac{\gamma}{\beta}+0.86[SA_{tot}]+0.63\frac{CS}{\beta}}, \tag{9}$$

$$\theta = 1+\frac{2[B]}{1.16[B]+0.46\frac{CS}{\beta}}\frac{[SA_{tot}]-[A_1B_1]}{[A_1B_1]}, \tag{10}$$

$$\theta' = \frac{\theta(2.22[A_1B_1]+0.86\frac{CS}{\beta})}{\sqrt{(1.11[A_1B_1]+0.43\frac{CS}{\beta})^2+1.12\theta[A_1B_1]^2+1.11[A_1B_1]+0.43\frac{CS}{\beta}}}, \tag{11}$$

169 In Eqs. 8 to 11, the four input variables (T (K), CS (s^{-1}), $[B]$ (m^{-3}), $[SA_{tot}]$ (m^{-3})) are shown in bold. Generally, only these four

170 variable parameters are needed for the 3-D chemical transport models. Additionally, compared with directly coupling cluster

171 dynamic simulations into 3-D chemical transport models, the parameterization of pseudo-steady-state $J_{1.4}$ requires much less

172 computational time.

2.2 Incorporating the Parameterization into Updated WRF-Chem/R2D-VBS Model

174 The updated parameterization of SA-DMA nucleation was incorporated in the WRF-Chem (Weather Research and Forecasting

175 model with Chemistry). Before adding the SA-DMA nucleation, we already incorporated seven other NPF mechanisms in the

176 model (Zhao et al., 2020): four inorganic pathways, including binary neutral/ion-induced SA-H$_2$O nucleation and ternary

177 neutral/ion-induced NH$_3$-SA-H$_2$O nucleation; and three organic pathways, including pure-organic neutral/ion-induced organic

178 nucleation and ternary nucleation involving organics and SA. The organic containing nucleation pathways are driven by ultra-

179 and extremely low volatility organic compounds (ULVOC and ELVOC) with O:C > 0.4, converted from monoterpene

180 autoxidation. The chemical transformation and volatility distribution of monoterpene is represented in the model by R2D-VBS

181 (Radical Two-Dimensional Volatility Basis Set framework) with constrained parameters against experiments. More details of

182 the R2D-VBS are given in our previous study (Zhao et al., 2020). The newly formed nano-sized particles and their initial size

183 evolution are accounted in the MOSAIC module by 20 size bins covering 1 nm to 10 μm. It is worth mentioning that the newly

184 formed particles from SA-DMA nucleation are lumped into a lower aerosol size bin in the model than that of other seven

185 pathways. This should be attributed to that our SA-DMA nucleation parameterization are formulated at a 1.4 nm-sized particle

186 formation rate while the remaining ones are fitted based on measured particle formation rates from CLOUD Chamber at a

187 mobility diameter of 1.7 nm. Given that condensation of gaseous SA and DMA on pre-existing aerosols and nucleation occur

188 simultaneously in real atmosphere, in the model, we then use a time-integrated-averaged concentration of precursors over each

189 time step to drive SA-DMA nucleation. The condensation sink for SA and DMA is calculated according to simulated real-

time PNSDs. In addition, the consumption of both SA and DMA concentration during nucleation is also accounted in the model, in order to represent a comprehensive sources-sink simulation scheme of two precursors in combination with other settings.

2.2.1 Sources and Sinks of Dimethylamine in the Updated WRF-Chem/R2D-VBS Model

A regional or global bottom-up emission inventory of DMA is currently lacking, mostly due to scarce direct measurements (Yang et al., 2022; Zhu et al., 2022). In previous 3D model studies, amine/NH_3 emission ratios have often been used to estimate amine emissions due to the close correlation between NH_3 and DMA emissions. However, a fixed amine/NH_3 ratio is likely to overestimate the concentrations of amines in rural areas while underestimating those in urban areas, where high concentrations of amines have been reported (Yao et al., 2018; Bergman et al., 2015). Here, a set of source-dependent DMA/NH_3 emission ratio was used to develop the emission inventory of DMA based on (Mao et al., 2018). The ratios for different emission sectors were determined by a source apportionment analysis, based on a simultaneous observation of NH_3, C1-C3 amines, NO_x, and SO_2 and also meteorological factors at a suburban site in Nanjing (Zheng et al., 2015a). We applied the source-dependent emission ratios (0.0070, 0.0018, 0.0015, 0.0100, and 0.0009 for chemical–industrial, other industrial, agricultural, residential, and transportation source types, respectively) to NH_3 emissions in the ABaCAS-EI 2017 (Emission Inventory of Air Benefit and Cost and Attainment Assessment System) for China mainland and the IIASA 2015 emission inventory for other areas to build continental DMA emission inventory (Zheng et al., 2019; Gao et al., 2020). In addition, DMA emission for maritime area was developed employing a DMA/NH_3 ratio derived from recent campaigns in offshore areas of China (see details in SI) (Chen et al., 2021a).

DMA can be removed from the atmosphere through three main pathways: gas-phase chemical reaction, aerosol uptake, and wet deposition, which are all explicitly considered in our model. For the gas-phase chemical reactions, only oxidation of DMA by •OH is included. Reactions with other oxidants (O_3 and NO_3) are much slower and therefore have negligible effects on DMA concentrations (Ge et al., 2011). The mechanism of DMA concentration depletion by aerosol uptake is still poorly understood, and the key parameter, uptake coefficient γ_u, varies in a wide range depending on many factors such as aerosol composition and relative humidity. In this study, we assumed $\gamma_u = 0.001$, approximately a median value among those reported by recent laboratory measurements (Qiu et al., 2011; Wang et al., 2010). Regarding DMA depletion by wet deposition, the treatment is similar to that of NH_3 based on Henry's Law. The key parameters for above sink processes are summarized in Table S2 in the *SI*.

2.2.2 Configuration of the Updated WRF-Chem/R2D-VBS Model.

The WRF-Chem model configured with the SA-DMA nucleation is applied to a domain covering eastern Asia with a horizontal resolution of 27 km, where Beijing is located close to the center. The simulations are performed for two winter months separately (December 2018 and January 2019) with 5 days spin-up run for each month. The ABaCAS-EI 2017 and IIASA 2015 emission inventory were used for China mainland and other areas, respectively. The biogenic emission is calculated by the Model of Emissions of Gases and Aerosols from Nature (MEGAN) v2.04 (Guenther et al., 2006). Except for the monoterpene-related gas and aerosol chemistry that is traced by R2D-VBS, the remaining gas- and aerosol chemical processes are simulated by the SAPRC99 gas chemistry scheme coupled with the MOSAIC (Model for Simulating Aerosol Interaction and Chemistry) aerosol module and a one-dimensional VBS set for SOA modeling (Zaveri et al., 2014; Shrivastava et al., 2019; Shrivastava et al., 2011).

Four scenario simulations with different configurations of the NPF mechanisms were conducted in this study to examine how the SA-DMA nucleation affects the simulations of aerosol size distribution: 1) 8 NPF mechanisms with the SA-DMA nucleation rate at 1.4 nm (abbr. DMA1.4_Mech8); 2) 8 NPF mechanisms with the SA-DMA nucleation rate at 1.7 nm

230 converted using modified Kerminen-Kulmala equation (Lehtinen et al., 2007) (DMA1.7_Mech8); 3) 7 NPF mechanisms

231 without the SA-DMA nucleation (NoDMA_Mech7); and 4) No NPF mechanism (NoDMA_Mech0). Among them, scenario 1

232 is our "best-case" with a full consideration of available nucleation mechanisms; scenario 2 is set to probe the feasibility to use

233 modified Kerminen-Kulmala equation to simulate the initial particle growth; scenario 3 is the "base-case" representing the

234 performance of the original model; and scenario 4 represents the evolution of aerosol population only contributed by primary

235 emission. Scenarios 3 and 4 were set as controlling groups to assess the role of SA-DMA nucleation and other mechanisms.

236 **2.3 Ambient Measurements**

237 Ambient observations were conducted at an urban site in Beijing from January 2018 to April 2018 and from October 2018 to

238 March 2019. The site is located on the West Campus of Beijing University of Chemical Technology. Details of the observation

239 site can be found in previous studies (Liu et al., 2020; Deng et al., 2020). The concentrations of SA and involving clusters are

240 measured using a chemical ionization high resolution time of flight mass spectrometer (CI-HTOF-MS) and a chemical

241 ionization time of flight mass spectrometer with a long mass analyzer (CI-LTOF-MS) (Bertram et al., 2011; Jokinen et al.,

242 2012). Other details in the sampling configurations have been reported in our previous study (Deng et al., 2020). Amine

243 concentrations are measured using a modified time of flight mass spectrometer (TOF-MS) (Zheng et al., 2015b; Cai et al.,

244 2021b). A weather station was deployed to measure the meteorological data, including ambient temperature, relative humidity

245 and pressure. The PNSDs of particles from 1 nm to 10 μm were measured using a particle size distribution (PSD) and a diethyl

246 glycol-scanning mobility particle sizer (DEG-SMPS) (Jiang et al., 2011; Liu et al., 2016; Cai et al., 2017a). CS is calculated

247 from the measured PNSDs and $J_{1.4}$ is calculated using an improved aerosol population balance formula (Cai and Jiang, 2017).

248 The details of instrument calibrations and data validations can be found in our previous study (Cai et al., 2021b).

249 **3 Results and discussion**

250 **3.1 Validation of Parameterization**

251 The reasonability of pseudo-steady-state assumptions in the SA-DMA nucleation pathway was tested through comparisons

252 between the e-folding time of cluster dynamics (τ) in the kinetic simulation (see details in the *SI*) and the time interval of

253 observational data (30 min in this study). The characteristic equilibrium time of involving clusters and simulated $J_{1.4}$ were

254 shown in Fig. S1 in the *SI*. Generally, in either clean and cold circumstances or polluted and warm circumstances, the

255 kinetically simulated $J_{1.4}$ could be well reproduced by parameterized pseudo-steady-state $J_{1.4}$. Actually, τ would vary greatly

256 with CoagS and γ, and would be higher on cleaner and colder days, while even in extremely clean and cold days with *CS* =

257 0.0001 s^{-1} and *T* = 255 K, τ of A_3B_3 (longer than other clusters) is only ~20 min, shorter than the data collection time interval

258 of 30 min. Thus for circumstances where there are high atmospheric concentrations of DMA and SA, such as most typical

259 polluted regions, we conclude that nucleation processes are rapid enough that kinetic $J_{1.4}$ can be represented by pseudo-steady-

260 state $J_{1.4}$.

261 Figure 1 presents the comparisons between parameterized $J_{1.4}$ in this study and those simulated in the kinetic models (hereafter

262 referred to as KM) presented by Cai et al. (2021) and the cluster dynamic simulations containing all A_mB_n (m, n≤4) clusters

263 (hereafter referred to as CDS). Generally, there are good consistencies the simulated $J_{1.4}$ between KM and the parameterization

264 with the correlation coefficient (R^2) and normalized mean bias (NMB) of 0.9297 and 0.16, respectively. The simulated $J_{1.4}$ in

265 KM can be reproduced by parameterized $J_{1.4}$ within a ±50% range for most of the cases in urban Beijing, with no systematic

266 deviations found between them.

267 Figure 1b shows that for most of the circumstances, deviations between the parameterized $J_{1.4}$ and $J_{1.4}$ simulated in CDS are

268 within a range of 1 order of magnitude. The R^2 and NMB of the simulated $J_{1.4}$ between this parameterization and CDS are

269   0.7244 and 0.29, respectively. However, for circumstances with high temperatures, the parameterized $J_{1.4}$ would be higher

270   than those simulated in CDS, which might be due to that the A_kB_k (k=2,3 and 4) clusters are assumed to be non-evaporative

271   in KM while they would evaporate back in CDS under high temperatures. The reasonability of cluster stability assumptions

272   under high temperatures relies mainly on the accuracy of quantum chemistry calculations, which requires more experimental

273   evidence and discussions. Additionally, due to the negative dependence of simulated $J_{1.4}$ on T, the simulated $J_{1.4}$ in this

274   parameterization would be mostly lower than 10 cm^{-3}s^{-1} under temperatures higher than 15 ℃, lower than the median and mean

275   value of particle formation rates measured during long-term observations in Beijing (Deng et al., 2021). Although they are

276   relatively higher than those simulated in CDS, the simulation results of NPF occurrence would not show large deviations.

277   The computational costs of these three simulations have also been tested on the same personal computer with a Matlab program.

278   To achieve the steady-state $J_{1.4}$ in a specific atmospheric condition, the CDS and KM needs ~10 s and ~0.05 s CPU time,

279   respectively, while the calculation of parameterized pseudo-steady-state $J_{1.4}$ merely costs ~2×10^{-7} s CPU time. The CPU time

280   was reduced by a factor of 5×10^7 and 4×10^4 compared to CDS and KM, respectively. Thus introducing this parameterization

281   into 3-D chemical transport models could greatly reduce the computational costs.

282   **3.2 The Dependence of Parameterized $J_{1.4}$ on Input Parameters**

283   The correlation between parameterized SA-DMA nucleation $J_{1.4}$ and the input parameters are shown in Fig. 2. The parameters

284   involved are T, CS, [DMA], and [SA$_{tot}$]. The mean values of measured data during the observation period (281K, 0.02 s^{-1}, 3

285   ppt, and 3.5×10^6 cm^{-3}, respectively) are applied as typical conditions in the base case. Different from the semi-empirical power-

286   law functions only based on precursor concentrations presented by Dunne et al. (2016), the dependences of particle formation

287   rates on T and CS are represented in our parameterizations. With T increasing from -10 to 20 ℃, γ would increase by ~2 orders

288   of magnitude, as shown in Fig. 2a, and thus $J_{1.4}$ would decrease by over 2 orders of magnitude. This should be attributed to

289   the positive dependence of evaporation rates of A_1B_1 clusters on the temperature. Under circumstances with high tempratures,

290   the formation of A_1B_1 and subsequent formation of larger clusters and 1.4 nm particles would be suppressed. The decreasing

291   trend of observed NPF rate ($J_{1.5}$ in this case) as a function of increasing T in urban Beijing has also been reported (Deng et al.,

292   2020), consistent with our parameterizations.

293   Fig. 2b shows that $J_{1.4}$ would decrease by 2-4 orders of magnitude with CS increasing by a factor of 10, and the logarithm

294   dependence is higher in circumstances with higher CS, such as urban Beijing, where CoagS dominates the sinks. This is

295   consistent with the negative CS dependence of measured particle formation rates and NPF occurrence demonstrated in previous

296   observations in Beijing (Deng et al., 2021; Cai et al., 2021b; Cai et al., 2021a). Note that the dependence of parameterized $J_{1.4}$

297   on CS is also sensitive to T due to the synergistic effect of evaporation and coagulation on the sink of A_1B_1 clusters, which are

298   the key species in SA-DMA nucleation (Cai et al., 2022). If temperatures are higher, evaporation would be the dominant sink

299   of A_1B_1 clusters while CS only suppresses the formation of larger clusters. While under lower temperatures, such as in

300   wintertime Beijing, CS would be the dominant sink of both A_1B_1 clusters and larger clusters.

301   The parameterized $J_{1.4}$ shows an increasing trend with increasing concentrations of SA and DMA. The parameterized $J_{1.4}$ is

302   approximately proportional to [SA]^4. This high dependence of parameterized $J_{1.4}$ on [SA] could well reproduce the

303   phenomenon that rapid formation of new particles usually occurs at noon, when there is usually strong formation of SA

304   molecules in the atmosphere. The dependence of $J_{1.4}$ on [DMA] is decreasing with increasing [DMA]. This is due to the near-

305   saturation formation of A_1B_1 clusters, which is also found in kinetic model simulation results (Cai et al., 2021d). Generally,

306   the parameterization could reproduce the fact that SA-DMA nucleation is driven by SA-DMA cluster formation, dominantly

307   suppressed by cluster evaporation and coagulation sinks.

3.3 Comparison of 3D Model Simulations with Observations

As [DMA], [SA] and CS are key input variables for the $J_{1.4}$ parameterization, we first compare simulated [DMA], [SA] and CS from the DMA1.4_Mech8 scenario with observations (Fig. 3). Generally, there are good consistencies of both mean values and temporal variations, although there are still deviations at certain times. The mean simulated [DMA], [SA], and CS are 1.9 ppt, 1.4×10^6 cm^{-3}, and 0.040 s^{-1}, respectively, close to observed values of 2.0 ppt, 1.6×10^6 cm^{-3}, and 0.043 s^{-1}. In a quantitative view, the R^2 between simulated and observed [DMA], [SA], and CS are 0.04, 0.37, and 0.40, respectively, while the coefficients during NPF periods increase to 0.12, 0.51, and 0.49. The normalized mean biases (NMBs) between simulated and observed [DMA], [SA], and CS are 4.5×10^{-3}, -0.22, and -0.36, respectively, while NMBs during NPF periods are -0.40, 0.01, and -0.66. Generally, the simulation of SA concentrations is good, especially during NPF periods with intense nucleation. We note that the correlation between simulated and observed DMA concentration is lower, which may be attributed to the large uncertainty of the diurnal variation of amine emission. Nevertheless, during NPF periods, the differences between the observed DMA concentration (0.78±0.60 ppt) and our simulation (1.10±0.60 ppt) is relatively small. For [SA] and CS, to which $J_{1.4}$ are most sensitive, we compare the timeseries of simulated and observed [SA]^4/CS^2 (based on the approximate dependence of $J_{1.4}$ on [SA] and CS, as shown in Fig. 2)during NPF periods to show the deviations of the combination of these two input parameters (Fig. S6). Generally, in most nucleation events, the simulated values would not deviate from the observed values by over an order of magnitude. This indicates the validity of the comprehensive representation of input parameters in the model.

The time series of PNSDs for different simulation scenarios are presented in Fig. 4. When SA-DMA nucleation is considered, the typical PNSDs shape in observed NPF days (12/07, 12/08, 12/09, 01/20, and 01/21), characterized as the burst of nanometer-sized particles and subsequent growth, are well captured by our "best-case" scenario DMA1.4_Mech8 and also DMA1.7_Mech8. By contrast, the scenarios without DMA-SA nucleation, NoDMA_Mech7 and NoDMA_Mech0, cannot reproduce the observed NPF events with a "vacancy band" for 1~10 nm size range over the entire simulation period. Actually, although there are slightly higher sub-3 nm particle concentrations in NoDMA_Mech7 than those in NoDMA_Mech0, which are generated from the 7 nucleation pathways other than DMA-SA nucleation, the newly formed particle concentrations are too low to survive in the subsequent growth and be separated from background aerosols in the PNSDs. These results demonstrate that SA-DMA nucleation should be the dominant mechanism during NPF events in Beijing compared with other 7 mechanisms.

Our results also reproduce the dependence of NPF occurrence on CS in Beijing. As shown in Fig. S2 in the *SI*, NPF generally occurs at low CS while high CS results in too low nucleation rates to initiate NPF. The results were also validated through comparison between the timeseries of the simulated and observed CS (Fig. 3c). Note that the simulated sub-3 nm particle concentrations also increase slightly on some non-NPF days in DMA1.4_Mech8 and DMA1.7_Mech8 scenarios, however, the concentrations are ~1 order of magnitude lower than those on NPF days and the newly formed particles also fail to survive in the subsequent growth. The improvements of using the nucleation parameterization in this study is further stressed in the comparison between DMA1.4_Mech8 scenario and the scenario (CLOUD) using the parameterization from Dunne et al. (2016). Figure S3 has shown that almost no rapid nucleation processes and NPF events are found in the simulation of CLOUD scenarios. In addition to the underestimation of nucleation rates, the simulated high nucleation rates usually occur on observed non-NPF days (Fig.S7), which should be attributed to the ignorance of CS dependence in the power-law function parameterizations.

Figure 5 further compares the simulated and observed PNSDs averaged over the simulation period. The "best-case" scenario DMA1.4_Mech8 brings the averaged PNSD in 1~200 nm size range much closer to the observation than those of "base-case" NoDMA_Mech7, and the latter only shows a minor change compared to scenario NoDMA_Mech0 without any nucleation. One may notice that the averaged PNSD in 2~10 nm size range for scenario DMA1.4_Mech8 is still lower than that of observation by ~1 order of magnitude, despite the good agreement in number concentrations of particles of ~1.4 nm. This

350 could be attributed to two possible reasons: the model underestimates the actual nucleation rates; or newly formed particles of

351 ~1.4 nm grow too fast to larger size bins in the model (> 10 nm). The first one can be excluded by a generally good agreement

352 between simulated nucleation rates and ones derived from observation, even with a slightly higher mean value for the former

353 (shown in next section, Fig. 6). The observation-simulation comparison of averaged PNSDs is further conducted for individual

354 NPF days. As shown in Fig. S8, the simulated PNSDs on all NPF days follow a similar pattern as the two-month-averaged one

355 in Fig. 6, indicating that nucleation in each simulated NPF day is accompanied by subsequent rapid growth. The difference in

356 the concentration of 2-10 nm particles between observation and simulation is therefore a common feature on various days and

357 is probably attributed to the simplified assumption in particle growth simulation. Hence, the gap in 2~10 nm size range might

358 be attributed to the particle growth simulations in the model which deserves further improvement. Moreover, in spite of similar

359 performance in improving PNSDs simulations compared to the "best-case" DMA1.4_Mech8, the scenario of DMA1.7_Mech8

360 presents a shifted PNSD pattern to larger size range. For these two scenarios including SA-DMA nucleation, scenario

361 DMA1.4_Mech8 is more reasonable since a systematic underestimation exists over the entire 1~10 nm range in scenario

362 DMA1.7_Mech8. Still, the conversion from 1.4 nm rate to those for larger particles through modified Kerminen-Kulmala

363 equation is an alternative way to depict SA-DMA nucleation for other models with different aerosol size settings.Overall,

364 despite aforementioned deficiencies, our updated WRF-Chem/R2D-VBS model configured with the SA-DMA nucleation

365 parameterization shows substantial improvement in representation of NPF events and the PNSD.

3.4 Contribution from Various Pathways to Nucleation Rates and Particle Number Concentrations

367 Quantitative analysis over various nucleation pathways is performed here to improve the understanding of NPF in Beijing. As

368 presented in Fig. 6, the variation of nucleation rates, which are derived from observed PNSD data, is well represented by the

369 best-case scenario DMA1.4_Mech8. Compared to the vast majority contribution from SA-DMA nucleation, the nucleation

370 rates from other nucleation mechanisms are lower by a factor of ~100. In addition, SA-DMA nucleation contributes over 60%

371 to aerosol population, reinforcing its dominant role in modulating aerosol population in urban atmosphere.

3.5 Sensitivity Analysis

373 Having shown the significant improvement of model performance in simulating NPF by coupling the SA-DMA nucleation

374 parameterization, we acknowledge that the simulation of SA-DMA nucleation in 3D model still has uncertainties in terms of

375 both source-sink representation of DMA and nucleation parameterization. Here, several key factors which may alter model

376 performance were selected to perform sensitivity analysis.

377 First, the uncertainties brought by ΔG achieved from different quantum chemistry results are tested for both parameterized $J_{1.4}$

378 and the 3-D chemical transport model simulations. In previous studies, a number of ΔG values have been reported: -11.02

379 kcal mol^{-1} (Ge et al., 2020b), -15.40 kcal mol^{-1} (Ortega et al., 2012), -13.54 kcal mol^{-1} (Myllys et al., 2019). The ΔG of -14.00

380 kcal mol^{-1} was applied in (Cai et al., 2021d) to achieve good consistencies between simulated and measured $J_{1.4}$ is also applied

381 in the sensitivity analysis. Figure S9 shows the variation of parameterized $J_{1.4}$ applying different ΔG values at 281 K, the

382 median temperature of the observation period. For DMA with median values of ~3 ppt, different $J_{1.4}$ could vary by ~5 orders

383 of magnitude with ΔG between -11.02 kcal mol^{-1} and -15.40 kcal mol^{-1}, while $J_{1.4}$ with ΔG of -13.54 kcal mol^{-1} is also lower

384 than that of -15.40 kcal mol^{-1} by a factor of ~10. However, if the DMA concentrations are up to ~30 ppt, the differences of $J_{1.4}$

385 when ΔG varies between -13.54 kcal mol^{-1} and -15.40 kcal mol^{-1} would become much smaller, due to the saturated formation

386 of A_1B_1 clusters. For the temperature of 298.15 K, the sensitivities of parameterized $J_{1.4}$ are relatively larger, because the

387 formation of A_1B_1 clusters is far from saturation. Generally, the parameterized $J_{1.4}$ could be very sensitive to different ΔG

388 values achieved from quantum chemistry results due to the essential influence of cluster stabilities. As a result, using a lower

389 ΔG value of -15.40 kcal mol^{-1} in the 3-D simulations with the DMA1.4_Mech8 scenario configuration could lead to much

390 higher nucleation rates compared to the observation (Fig. S10). Thus we call for a more systematic performance assessment
391 of quantum chemistry calculation methods to constrain the uncertainties of cluster thermodynamic stabilities.

392 Moreover, for the DMA source, we conduct two sensitivity scenarios of doubling (DMA2) and halving (DMA0.5) the inputted
393 DMA emission to test the influence of limited measurements in constraining the DMA/NH_3 emission ratio. As for the three
394 sink processes, the parameters for DMA-•OH reaction and wet deposition reported in the literature have relatively small
395 differences while aerosol uptake coefficient of DMA covers a wide range over two orders of magnitude. We then conduct two
396 sensitivity scenarios using the upper (4.4×10^{-2}, Upt4.4E-2) and lower (5.9×10^{-4}, Upt5.9E-4) limit of aerosol uptake coefficient.
397 All sensitivity scenarios are on the basis of the DMA1.4_Mech8 configuration. The influence of scaled DMA emissions and
398 varying uptake coefficients on simulated DMA concentration, PNSDs, and nucleation rate is shown in Fig. S11-S21 in the *SI*.
399 As expected, the DMA concentration, especially for the nighttime spikes, is sensitive to the emission change. In DMA0.5, the
400 simulated *J* are lower than those observed in almost all cases. In contrast, although the simulated *J* in DMA2 is on average
401 higher than observations, they are comparable in some specific cases. Considering that during NPF cases, the observed [DMA]
402 are averagely 1.4 times higher than those simulated in DMA1.4_Mech8, we propose that the slight underestimation of DMA
403 concentrations in this case might be the reason for underestimation in *J* in some cases. The sensitivity analysis for the uptake
404 coefficient, however, shows different results. A higher uptake coefficient of 4.4×10^{-2} leads to a much lower DMA
405 concentration (10% of the "best-case") while DMA concentration only increase slightly when the lower limit of 5.9×10^{-4} is
406 used. Moreover, the change in uptake coefficient show limited effect on PNSD. The reason is that the DMA concentrations
407 during NPF periods are much less affected by the changes in uptake coefficient than those in non-NPF periods, since NPF
408 usually occurs at low CS conditions when the uptake of DMA is weak.

409 The sensitivity analysis above show that the parameters used in our simulation are reasonable, since perturbations within the
410 ranges reported in the literature generally worsen the model performance. We also expect more field measurements of DMA
411 emission and its aerosol uptake to further constrain the key source-sink process parameters in the simulation of DMA, although
412 some of them show minor effect on NPF and PNSD simulations.

413 **4 Conclusions**

414 This study presents a SA-DMA nucleation parameterization for application in 3-D chemical transport models. Compared to
415 semi-empirical power-law fitting parameterizations, this new parameterization is based on the key pathway of SA-DMA
416 cluster formation and make good representations of the coagulation scavenging effect and cluster stability. Pseudo-steady-
417 state assumptions are applied and validated according to the short characteristic equilibrium time and through comparisons
418 with the cluster dynamic simulations and the kinetic model. Compared with simulating the SA-DMA nucleation with cluster
419 dynamic simulations or the kinetic model, applying this parameterization into 3-D chemical transport models would greatly
420 reduce the computational costs.

421 We incorporate this new parameterization as well as the sources and sinks of DMA into the WRF-Chem/R2D-VBS model.
422 Using the updated model, we simulate the DMA concentrations and PNSDs in Beijing during December 2018 and January
423 2019. Comparisons are made between 3-D model simulations and ambient measurements. Good consistency is achieved in
424 simulating the precursor concentrations, which validates the source-sink simulation of SA and DMA. Primarily, our
425 quantitative analysis show that compared to other nucleation mechanisms, SA-DMA nucleation would contribute to >99% of
426 particle formation rates and >60% of particle number concentrations during the simulation period in urban Beijing. Although
427 the uncertainties exist due to the excess rapid growth in 3-D simulation, SA-DMA nucleation should be dominant sources of
428 aerosol population due to its dominance in new particle formation rates. Furtherly, the 3-D simulations with this
429 parameterization make good predictions of the CS-dependent NPF occurrence in urban Beijing and quantitatively reproduce

430 the particle size distributions. These demonstrate that incorporating the SA-DMA nucleation parameterization including the

431 effect of coagulation scavenging and cluster stabilities with 3-D chemical transport models would significantly improve the

432 simulation of NPF and the particle size distributions. Such improvement would be important for further simulations of cloud

433 condensation nuclei and the climate effects of aerosols and NPF events. The improved simulations of particle size distributions

434 also provide more evidence for quantitatively evaluate the environmental and health effect of ultrafine particles.

435 This study has emphasized that 3-D simulations with this new parameterization could reproduce the CS-dependent particle

436 formation rates and NPF occurrence in Beijing. As CS could vary in a relative wide range between NPF days and non-NPF

437 days in urban atmosphere (Xiao et al., 2015; Wu et al., 2007; Deng et al., 2021), compared to semi-empirical power-law

438 functions, this parameterization of particle formation rates would be more effective in predicting the NPF occurrence in urban

439 atmosphere. Additionally, the particle formation rates from other nucleation mechanisms should also be suppressed by high

440 CS, which needs further exploration and parameterizations. Our methodology of applying pseudo-steady-state assumptions to

441 kinetic models could be important in reducing computational costs of other SA-amine nucleation systems. For instance,

442 quantum chemistry calculations also indicate that other basic molecules like trimethylamine and diamines (Jen et al., 2016;

443 Jen et al., 2014a), might also form relative stable clusters with SA molecules, hence the methodology of parameterizations in

444 this study could also be extended for them, or the basic molecules could also be treated as equivalent DMA concentrations.

445 Note that although some studies have revealed that SA-DMA nucleation could also be enhanced by adding other molecules in

446 certain conditions, quantitative analysis of these effects in relevant atmospheric conditions is still lacking, thus in this study,

447 we set up this parameterization only based on SA-DMA binary nucleation.

448 **Codes/Data availability**

449 The simulation output data and codes needed for figure reproduction have been posted on Github. The link is

450 https://github.com/laoyeyelao/new-SA-DMA-parameterization.git.

451 **Author Contribution**

452 Y.L., J.S., B.Z., and J.J. designed the research; J.Z., M.K., and J.J. collected the observational data; Y.L., R.C., and J.J. set up

453 and tested the parameterization; J.S., B.Z., S.W., and D.G. developed the 3-D model and performed the simulations; Y.L. and

454 J.S. analyzed the data with the help of R.C., B.Z., and J.J.; M.S. and Y.G. presented important suggestions for the writings;

455 Y.L., J.S., B.Z., and J.J. wrote the paper with inputs from all co-authors.

456 **Competing Interests**

457 Some authors are members of the editorial board of journal *Atmospheric Chemistry and Physics*. The peer-review process was

458 guided by an independent editor, and the authors have also no other competing interests to declare.

459 **Acknowledgement**

460 Financial support from the National Natural Science Foundation of China (22188102 and 42275110), Tencent Foundation

461 through the XPLORER PRIZE and Samsung $PM_{2.5}$ SRP are acknowledged. M. Shrivastava acknowledges the support from

462 the U.S. Department of Energy (DOE), Office of Science, Office of Biological and Environmental Research through the

463 Early Career Research Program.

464   **References**

465   Almeida, J., Schobesberger, S., Kurten, A., Ortega, I. K., Kupiainen-Maatta, O., Praplan, A. P., Adamov, A., Amorim, A.,
466   Bianchi, F., Breitenlechner, M., David, A., Dommen, J., Donahue, N. M., Downard, A., Dunne, E., Duplissy, J., Ehrhart,
467   S., Flagan, R. C., Franchin, A., Guida, R., Hakala, J., Hansel, A., Heinritzi, M., Henschel, H., Jokinen, T., Junninen, H.,
468   Kajos, M., Kangasluoma, J., Keskinen, H., Kupc, A., Kurten, T., Kvashin, A. N., Laaksonen, A., Lehtipalo, K., Leiminger,
469   M., Leppa, J., Loukonen, V., Makhmutov, V., Mathot, S., McGrath, M. J., Nieminen, T., Olenius, T., Onnela, A., Petaja,
470   T., Riccobono, F., Riipinen, I., Rissanen, M., Rondo, L., Ruuskanen, T., Santos, F. D., Sarnela, N., Schallhart, S.,
471   Schnitzhofer, R., Seinfeld, J. H., Simon, M., Sipila, M., Stozhkov, Y., Stratmann, F., Tome, A., Trostl, J., Tsagkogeorgas,
472   G., Vaattovaara, P., Viisanen, Y., Virtanen, A., Vrtala, A., Wagner, P. E., Weingartner, E., Wex, H., Williamson, C.,
473   Wimmer, D., Ye, P. L., Yli-Juuti, T., Carslaw, K. S., Kulmala, M., Curtius, J., Baltensperger, U., Worsnop, D. R.,
474   Vehkamaki, H., and Kirkby, J.: Molecular understanding of sulphuric acid-amine particle nucleation in the atmosphere,
475   Nature, 502, 359-363, 2013.
476   Bergman, T., Laaksonen, A., Korhonen, H., Malila, J., Dunne, E. M., Mielonen, T., Lehtinen, K. E. J., Kuhn, T., Arola, A.,
477   and Kokkola, H.: Geographical and diurnal features of amine-enhanced boundary layer nucleation, J Geophys Res-Atmos,
478   120, 9606-9624, 2015.
479   Bertram, T. H., Kimmel, J. R., Crisp, T. A., Ryder, O. S., Yatavelli, R. L. N., Thornton, J. A., Cubison, M. J., Gonin, M., and
480   Worsnop, D. R.: A field-deployable, chemical ionization time-of-flight mass spectrometer, Atmos. Meas. Tech., 4, 1471-
481   1479, 10.5194/amt-4-1471-2011, 2011.
482   Cai, R., Chen, D.-R., Hao, J., and Jiang, J.: A miniature cylindrical differential mobility analyzer for sub-3 nm particle sizing,
483   Journal of Aerosol Science, 106, 111-119, https://doi.org/10.1016/j.jaerosci.2017.01.004, 2017a.
484   Cai, R., Yan, C., Worsnop, D. R., Bianchi, F., Kerminen, V.-M., Liu, Y., Wang, L., Zheng, J., Kulmala, M., and Jiang, J.: An
485   indicator for sulfuric acid–amine nucleation in atmospheric environments, Aerosol Science and Technology, 55, 1059-
486   1069, 10.1080/02786826.2021.1922598, 2021a.
487   Cai, R., Yan, C., Yang, D., Yin, R., Lu, Y., Deng, C., Fu, Y., Ruan, J., Li, X., Kontkanen, J., Zhang, Q., Kangasluoma, J., Ma,
488   Y., Hao, J., Worsnop, D. R., Bianchi, F., Paasonen, P., Kerminen, V.-M., Liu, Y., Wang, L., Zheng, J., Kulmala, M., and
489   Jiang, J.: Sulfuric acid–amine nucleation in urban Beijing, Atmospheric Chemistry and Physics, 21, 2457-2468,
490   10.5194/acp-21-2457-2021, 2021b.
491   Cai, R. L. and Jiang, J. K.: A new balance formula to estimate new particle formation rate: reevaluating the effect of coagulation
492   scavenging, Atmos Chem Phys, 17, 12659-12675, 2017.
493   Cai, R. L., Yang, D. S., Fu, Y. Y., Wang, X., Li, X. X., Ma, Y., Hao, J. M., Zheng, J., and Jiang, J. K.: Aerosol surface area
494   concentration: a governing factor in new particle formation in Beijing, Atmos Chem Phys, 17, 12327-12340, 2017b.
495   Cai, R. L., Yan, C., Worsnop, D. R., Bianchi, F., Kerminen, V. M., Liu, Y. C., Wang, L., Zheng, J., Kulmala, M., and Jiang,
496   J. K.: An indicator for sulfuric acid-amine nucleation in atmospheric environments, Aerosol Sci Tech, 55, 1059-1069,
497   2021c.
498   Cai, R. L., Yan, C., Yang, D. S., Yin, R. J., Lu, Y. Q., Deng, C. J., Fu, Y. Y., Ruan, J. X., Li, X. X., Kontkanen, J., Zhang, Q.,
499   Kangasluoma, J., Ma, Y., Hao, J. M., Worsnop, D. R., Bianchi, F., Paasonen, P., Kerminen, V. M., Liu, Y. C., Wang, L.,
500   Zheng, J., Kulmala, M., and Jiang, J. K.: Sulfuric acid-amine nucleation in urban Beijing, Atmos Chem Phys, 21, 2457-
501   2468, 2021d.
502   Cai, R. L., Yin, R. J., Yan, C., Yang, D. S., Deng, C. J., Dada, L., Kangasluoma, J., Kontkanen, J., Halonen, R., Ma, Y., Zhang,
503   X. H., Paasonen, P., Petaja, T., Kerminen, V. M., Liu, Y. C., Bianchi, F., Zheng, J., Wang, L., Hao, J. M., Smith, J. N.,
504   Donahue, N. M., Kulmala, M., Worsnop, D. R., and Jiang, J. K.: The missing base molecules in atmospheric acid-base
505   nucleation, Natl Sci Rev, 9, 2022.
506   Chan, T. W. and Mozurkewich, M.: Measurement of the coagulation rate constant for sulfuric acid particles as a function of
507   particle size using tandem differential mobility analysis, J Aerosol Sci, 32, 321-339, 2001.
508   Chen, D., Shen, Y., Wang, J., Gao, Y., Gao, H., and Yao, X.: Mapping gaseous dimethylamine, trimethylamine, ammonia,
509   and their particulate counterparts in marine atmospheres of China's marginal seas – Part 1: Differentiating marine
510   emission from continental transport, Atmos Chem Phys, 21, 16413-16425, 10.5194/acp-21-16413-2021, 2021a.
511   Chen, M., Titcombe, M., Jiang, J., Jen, C., Kuang, C., Fischer, M. L., Eisele, F. L., Siepmann, J. I., Hanson, D. R., Zhao, J.,
512   and McMurry, P. H.: Acid-base chemical reaction model for nucleation rates in the polluted atmospheric boundary layer,
513   Proc Natl Acad Sci U S A, 109, 18713-18718, 10.1073/pnas.1210285109, 2012.
514   Chen, X., Yang, W., Wang, Z., Li, J., Hu, M., An, J., Wu, Q., Wang, Z., Chen, H., Wei, Y., Du, H., and Wang, D.: Improving
515   new particle formation simulation by coupling a volatility-basis set (VBS) organic aerosol module in NAQPMS+APM,
516   Atmos Environ, 204, 1-11, https://doi.org/10.1016/j.atmosenv.2019.01.053, 2019.
517   Chen, X., Yu, F., Yang, W., Sun, Y., Chen, H., Du, W., Zhao, J., Wei, Y., Wei, L., Du, H., Wang, Z., Wu, Q., Li, J., An, J.,
518   and Wang, Z.: Global–regional nested simulation of particle number concentration by combing microphysical processes
519   with an evolving organic aerosol module, Atmos. Chem. Phys., 21, 9343-9366, 10.5194/acp-21-9343-2021, 2021b.
520   Deng, C., Cai, R., Yan, C., Zheng, J., and Jiang, J.: Formation and growth of sub-3 nm particles in megacities: impact of
521   background aerosols, Faraday Discuss, 226, 348-363, 10.1039/d0fd00083c, 2021.
522   Deng, C. J., Fu, Y. Y., Dada, L., Yan, C., Cai, R. L., Yang, D. S., Zhou, Y., Yin, R. J., Lu, Y. Q., Li, X. X., Qiao, X. H., Fan,
523   X. L., Nie, W., Kontkanen, J., Kangasluoma, J., Chu, B. W., Ding, A. J., Kerminen, V. M., Paasonen, P., Worsnop, D.
524   R., Bianchi, F., Liu, Y. C., Zheng, J., Wang, L., Kulmala, M., and Jiang, J. K.: Seasonal Characteristics of New Particle
525   Formation and Growth in Urban Beijing, Environ Sci Technol, 54, 8547-8557, 2020.

Dunne, E. M., Gordon, H., Kurten, A., Almeida, J., Duplissy, J., Williamson, C., Ortega, I. K., Pringle, K. J., Adamov, A., Baltensperger, U., Barmet, P., Benduhn, F., Bianchi, F., Breitenlechner, M., Clarke, A., Curtius, J., Dommen, J., Donahue, N. M., Ehrhart, S., Flagan, R. C., Franchin, A., Guida, R., Hakala, J., Hansel, A., Heinritzi, M., Jokinen, T., Kangasluoma, J., Kirkby, J., Kulmala, M., Kupc, A., Lawler, M. J., Lehtipalo, K., Makhmutov, V., Mann, G., Mathot, S., Merikanto, J., Miettinen, P., Nenes, A., Onnela, A., Rap, A., Reddington, C. L. S., Riccobono, F., Richards, N. A. D., Rissanen, M. P., Rondo, L., Sarnela, N., Schobesberger, S., Sengupta, K., Simon, M., Sipilaa, M., Smith, J. N., Stozhkov, Y., Tome, A., Trostl, J., Wagner, P. E., Wimmer, D., Winkler, P. M., Worsnop, D. R., and Carslaw, K. S.: Global atmospheric particle formation from CERN CLOUD measurements, Science, 354, 1119-1124, 2016.

Gao, M., Han, Z., Tao, Z., Li, J., Kang, J.-E., Huang, K., Dong, X., Zhuang, B., Li, S., Ge, B., Wu, Q., Lee, H.-J., Kim, C.-H., Fu, J. S., Wang, T., Chin, M., Li, M., Woo, J.-H., Zhang, Q., Cheng, Y., Wang, Z., and Carmichael, G. R.: Air quality and climate change, Topic 3 of the Model Inter-Comparison Study for Asia Phase III (MICS-Asia III) – Part 2: aerosol radiative effects and aerosol feedbacks, Atmospheric Chemistry and Physics, 20, 1147-1161, 10.5194/acp-20-1147-2020, 2020.

Ge, P., Luo, G., Huang, W., Xie, H., Chen, J., and Luo, Y.: Theoretical study of the hydration effects on alkylamine and alkanolamine clusters and the atmospheric implication, Chemosphere, 243, 125323, https://doi.org/10.1016/j.chemosphere.2019.125323, 2020a.

Ge, P., Luo, G., Huang, W., Xie, H. B., Chen, J. W., and Luo, Y.: Theoretical study of the hydration effects on alkylamine and alkanolamine clusters and the atmospheric implication, Chemosphere, 243, 2020b.

Ge, X., Wexler, A. S., and Clegg, S. L.: Atmospheric amines – Part I. A review, Atmos Environ, 45, 524-546, 10.1016/j.atmosenv.2010.10.012, 2011.

Glasoe, W. A., Volz, K., Panta, B., Freshour, N., Bachman, R., Hanson, D. R., McMurry, P. H., and Jen, C.: Sulfuric acid nucleation: An experimental study of the effect of seven bases, J Geophys Res-Atmos, 120, 1933-1950, 2015.

Gordon, H., Kirkby, J., Baltensperger, U., Bianchi, F., Breitenlechner, M., Curtius, J., Dias, A., Dommen, J., Donahue, N. M., Dunne, E. M., Duplissy, J., Ehrhart, S., Flagan, R. C., Frege, C., Fuchs, C., Hansel, A., Hoyle, C. R., Kulmala, M., Kurten, A., Lehtipalo, K., Makhmutov, V., Molteni, U., Rissanen, M. P., Stozhkov, Y., Trostl, J., Tsagkogeorgas, G., Wagner, R., Williamson, C., Wimmer, D., Winkler, P. M., Yan, C., and Carslaw, K. S.: Causes and importance of new particle formation in the present-day and preindustrial atmospheres, J Geophys Res-Atmos, 122, 8739-8760, 2017.

Guenther, A., Karl, T., Harley, P., Wiedinmyer, C., Palmer, P. I., and Geron, C.: Estimates of global terrestrial isoprene emissions using MEGAN (Model of Emissions of Gases and Aerosols from Nature), Atmos. Chem. Phys., 6, 3181-3210, 10.5194/acp-6-3181-2006, 2006.

Hanson, D. R., Bier, I., Panta, B., Jen, C. N., and McMurry, P. H.: Computational Fluid Dynamics Studies of a Flow Reactor: Free Energies of Clusters of Sulfuric Acid with NH3 or Dimethyl Amine, J Phys Chem A, 121, 3976-3990, 2017.

Jen, C. N., McMurry, P. H., and Hanson, D. R.: Stabilization of sulfuric acid dimers by ammonia, methylamine, dimethylamine, and trimethylamine, Journal of Geophysical Research: Atmospheres, 119, 7502-7514, 10.1002/2014jd021592, 2014a.

Jen, C. N., McMurry, P. H., and Hanson, D. R.: Stabilization of sulfuric acid dimers by ammonia, methylamine, dimethylamine, and trimethylamine, J Geophys Res-Atmos, 119, 7502-7514, 2014b.

Jen, C. N., Bachman, R., Zhao, J., McMurry, P. H., and Hanson, D. R.: Diamine-sulfuric acid reactions are a potent source of new particle formation, Geophys Res Lett, 43, 867-873, 10.1002/2015gl066958, 2016.

Jiang, J., Chen, M., Kuang, C., Attoui, M., and McMurry, P. H.: Electrical Mobility Spectrometer Using a Diethylene Glycol Condensation Particle Counter for Measurement of Aerosol Size Distributions Down to 1 nm, Aerosol Science and Technology, 45, 510-521, 10.1080/02786826.2010.547538, 2011.

Jokinen, T., Sipilä, M., Junninen, H., Ehn, M., Lönn, G., Hakala, J., Petäjä, T., Mauldin Iii, R. L., Kulmala, M., and Worsnop, D. R.: Atmospheric sulphuric acid and neutral cluster measurements using CI-APi-TOF, Atmos. Chem. Phys., 12, 4117-4125, 10.5194/acp-12-4117-2012, 2012.

Kulmala, M.: How particles nucleate and grow, Science, 302, 1000-1001, 2003.

Kulmala, M., Vehkamaki, H., Petaja, T., Dal Maso, M., Lauri, A., Kerminen, V. M., Birmili, W., and McMurry, P. H.: Formation and growth rates of ultrafine atmospheric particles: a review of observations, J Aerosol Sci, 35, 143-176, 2004.

Kurten, A., Li, C. X., Bianchi, F., Curtius, J., Dias, A., Donahue, N. M., Duplissy, J., Flagan, R. C., Hakala, J., Jokinen, T., Kirkby, J., Kulmala, M., Laaksonen, A., Lehtipalo, K., Makhmutov, V., Onnela, A., Rissanen, M. P., Simon, M., Sipila, M., Stozhkov, Y., Trostl, J., Ye, P. L., and McMurry, P. H.: New particle formation in the sulfuric acid-dimethylamine-water system: reevaluation of CLOUD chamber measurements and comparison to an aerosol nucleation and growth model, Atmos Chem Phys, 18, 845-863, 2018.

Kurten, A., Jokinen, T., Simon, M., Sipila, M., Sarnela, N., Junninen, H., Adamov, A., Almeida, J., Amorim, A., Bianchi, F., Breitenlechner, M., Dommen, J., Donahue, N. M., Duplissy, J., Ehrhart, S., Flagan, R. C., Franchin, A., Hakala, J., Hansel, A., Heinritzi, M., Hutterli, M., Kangasluoma, J., Kirkby, J., Laaksonen, A., Lehtipalo, K., Leiminger, M., Makhmutov, V., Mathot, S., Onnela, A., Petaja, T., Praplan, A. P., Riccobono, F., Rissanen, M. P., Rondo, L., Schobesberger, S., Seinfeld, J. H., Steiner, G., Tome, A., Trostl, J., Winkler, P. M., Williamson, C., Wimmer, D., Ye, P. L., Baltensperger, U., Carslaw, K. S., Kulmala, M., Worsnop, D. R., and Curtius, J.: Neutral molecular cluster formation of sulfuric acid-dimethylamine observed in real time under atmospheric conditions, P Natl Acad Sci USA, 111, 15019-15024, 2014.

Lehtinen, K. E. J., Dal Maso, M., Kulmala, M., and Kerminen, V. M.: Estimating nucleation rates from apparent particle formation rates and vice versa: Revised formulation of the Kerminen-Kulmala equation, J Aerosol Sci, 38, 988-994, 2007.

Lehtipalo, K., Rondo, L., Kontkanen, J., Schobesberger, S., Jokinen, T., Sarnela, N., Kurten, A., Ehrhart, S., Franchin, A., Nieminen, T., Riccobono, F., Sipila, M., Yli-Juuti, T., Duplissy, J., Adamov, A., Ahlm, L., Almeida, J., Amorim, A., Bianchi, F., Breitenlechner, M., Dommen, J., Downard, A. J., Dunne, E. M., Flagan, R. C., Guida, R., Hakala, J., Hansel,

A., Jud, W., Kangasluoma, J., Kerminen, V. M., Keskinen, H., Kim, J., Kirkby, J., Kupc, A., Kupiainen-Maatta, O., Laaksonen, A., Lawler, M. J., Leiminger, M., Mathot, S., Olenius, T., Ortega, I. K., Onnela, A., Petaja, T., Praplan, A., Rissanen, M. P., Ruuskanen, T., Santos, F. D., Schallhart, S., Schnitzhofer, R., Simon, M., Smith, J. N., Trostl, J., Tsagkogeorgas, G., Tome, A., Vaattovaara, P., Vehkamaki, H., Vrtala, A. E., Wagner, P. E., Williamson, C., Wimmer, D., Winkler, P. M., Virtanen, A., Donahue, N. M., Carslaw, K. S., Baltensperger, U., Riipinen, I., Curtius, J., Worsnop, D. R., and Kulmala, M.: The effect of acid-base clustering and ions on the growth of atmospheric nano-particles, Nat Commun, 7, 2016.

Liu, J., Jiang, J., Zhang, Q., Deng, J., and Hao, J.: A spectrometer for measuring particle size distributions in the range of 3 nm to 10 μm, Frontiers of Environmental Science & Engineering, 10, 63-72, 10.1007/s11783-014-0754-x, 2016.

Liu, L., Yu, F., Du, L., Yang, Z., Francisco, J. S., and Zhang, X.: Rapid sulfuric acid–dimethylamine nucleation enhanced by nitric acid in polluted regions, Proceedings of the National Academy of Sciences, 118, e2108384118, 10.1073/pnas.2108384118, 2021.

Liu, Y., Yan, C., Feng, Z., Zheng, F., Fan, X., Zhang, Y., Li, C., Zhou, Y., Lin, Z., Guo, Y., Zhang, Y., Ma, L., Zhou, W., Liu, Z., Dada, L., Dällenbach, K., Kontkanen, J., Cai, R., Chan, T., Chu, B., Du, W., Yao, L., Wang, Y., Cai, J., Kangasluoma, J., Kokkonen, T., Kujansuu, J., Rusanen, A., Deng, C., Fu, Y., Yin, R., Li, X., Lu, Y., Liu, Y., Lian, C., Yang, D., Wang, W., Ge, M., Wang, Y., Worsnop, D. R., Junninen, H., He, H., Kerminen, V.-M., Zheng, J., Wang, L., Jiang, J., Petäjä, T., Bianchi, F., and Kulmala, M.: Continuous and comprehensive atmospheric observations in Beijing: a station to understand the complex urban atmospheric environment, Big Earth Data, 4, 295-321, 10.1080/20964471.2020.1798707, 2020.

Lu, Y. Q., Liu, L., Ning, A., Yang, G., Liu, Y. L., Kurten, T., Vehkamaki, H., Zhang, X. H., and Wang, L.: Atmospheric Sulfuric Acid-Dimethylamine Nucleation Enhanced by Trifluoroacetic Acid, Geophys Res Lett, 47, 2020.

Mao, J., Yu, F., Zhang, Y., An, J., Wang, L., Zheng, J., Yao, L., Luo, G., Ma, W., Yu, Q., Huang, C., Li, L., and Chen, L.: High-resolution modeling of gaseous methylamines over a polluted region in China: source-dependent emissions and implications of spatial variations, Atmospheric Chemistry and Physics, 18, 7933-7950, 10.5194/acp-18-7933-2018, 2018.

Marten, R., Xiao, M., Rörup, B., Wang, M., Kong, W., He, X.-C., Stolzenburg, D., Pfeifer, J., Marie, G., Wang, D. S., Scholz, W., Baccarini, A., Lee, C. P., Amorim, A., Baalbaki, R., Bell, D. M., Bertozzi, B., Caudillo, L., Chu, B., Dada, L., Duplissy, J., Finkenzeller, H., Carracedo, L. G., Granzin, M., Hansel, A., Heinritzi, M., Hofbauer, V., Kemppainen, D., Kürten, A., Lampimäki, M., Lehtipalo, K., Makhmutov, V., Manninen, H. E., Mentler, B., Petäjä, T., Philippov, M., Shen, J., Simon, M., Stozhkov, Y., Tomé, A., Wagner, A. C., Wang, Y., Weber, S. K., Wu, Y., Zauner-Wieczorek, M., Curtius, J., Kulmala, M., Möhler, O., Volkamer, R., Winkler, P. M., Worsnop, D. R., Dommen, J., Flagan, R. C., Kirkby, J., Donahue, N. M., Lamkaddam, H., Baltensperger, U., and El Haddad, I.: Survival of newly formed particles in haze conditions, Environmental Science: Atmospheres, 2, 491-499, 10.1039/D2EA00007E, 2022.

McGrath, M. J., Olenius, T., Ortega, I. K., Loukonen, V., Paasonen, P., Kurten, T., Kulmala, M., and Vehkamaki, H.: Atmospheric Cluster Dynamics Code: a flexible method for solution of the birth-death equations, Atmos Chem Phys, 12, 2345-2355, 2012.

Merikanto, J., Spracklen, D. V., Mann, G. W., Pickering, S. J., and Carslaw, K. S.: Impact of nucleation on global CCN, Atmos Chem Phys, 9, 8601-8616, 2009.

Myllys, N., Kubecka, J., Besel, V., Alfaouri, D., Olenius, T., Smith, J. N., and Passananti, M.: Role of base strength, cluster structure and charge in sulfuric-acid-driven particle formation, Atmos Chem Phys, 19, 9753-9768, 2019.

Olenius, T., Kupiainen-Maatta, O., Ortega, I. K., Kurten, T., and Vehkamaki, H.: Free energy barrier in the growth of sulfuric acid-ammonia and sulfuric acid-dimethylamine clusters, J Chem Phys, 139, 2013.

Olenius, T., Halonen, R., Kurten, T., Henschel, H., Kupiainen-Maata, O., Ortega, I. K., Jen, C. N., Vehkamaki, H., and Riipinen, I.: New particle formation from sulfuric acid and amines: Comparison of monomethylamine, dimethylamine, and trimethylamine, J Geophys Res-Atmos, 122, 7103-7118, 2017.

Ortega, I. K., Kupiainen, O., Kurten, T., Olenius, T., Wilkman, O., McGrath, M. J., Loukonen, V., and Vehkamaki, H.: From quantum chemical formation free energies to evaporation rates, Atmos Chem Phys, 12, 225-235, 2012.

Qiu, C., Wang, L., Lal, V., Khalizov, A. F., and Zhang, R.: Heterogeneous reactions of alkylamines with ammonium sulfate and ammonium bisulfate, Environ Sci Technol, 45, 4748-4755, 10.1021/es1043112, 2011.

Riccobono, F., Schobesberger, S., Scott, C. E., Dommen, J., Ortega, I. K., Rondo, L., Almeida, J., Amorim, A., Bianchi, F., Breitenlechner, M., David, A., Downard, A., Dunne, E. M., Duplissy, J., Ehrhart, S., Flagan, R. C., Franchin, A., Hansel, A., Junninen, H., Kajos, M., Keskinen, H., Kupc, A., Kurten, A., Kvashin, A. N., Laaksonen, A., Lehtipalo, K., Makhmutov, V., Mathot, S., Nieminen, T., Onnela, A., Petaja, T., Praplan, A. P., Santos, F. D., Schallhart, S., Seinfeld, J. H., Sipila, M., Spracklen, D. V., Stozhkov, Y., Stratmann, F., Tome, A., Tsagkogeorgas, G., Vaattovaara, P., Viisanen, Y., Vrtala, A., Wagner, P. E., Weingartner, E., Wex, H., Wimmer, D., Carslaw, K. S., Curtius, J., Donahue, N. M., Kirkby, J., Kulmala, M., Worsnop, D. R., and Baltensperger, U.: Oxidation Products of Biogenic Emissions Contribute to Nucleation of Atmospheric Particles, Science, 344, 717-721, 2014.

Sceats, M. G.: Brownian coagulation in aerosols—the role of long range forces, J Colloid Interf Sci, 129, 105-112, https://doi.org/10.1016/0021-9797(89)90419-0, 1989.

Seinfeld, J. H. and Pandis, S. N.: Atmospheric Chemistry and Physics: From Air Pollution to Climate Change, 1998.

Semeniuk, K. and Dastoor, A.: Current state of aerosol nucleation parameterizations for air-quality and climate modeling, Atmos Environ, 179, 77-106, 2018.

Shrivastava, M., Fast, J., Easter, R., Gustafson Jr, W. I., Zaveri, R. A., Jimenez, J. L., Saide, P., and Hodzic, A.: Modeling organic aerosols in a megacity: comparison of simple and complex representations of the volatility basis set approach, Atmos. Chem. Phys., 11, 6639-6662, 10.5194/acp-11-6639-2011, 2011.

653 Shrivastava, M., Andreae, M. O., Artaxo, P., Barbosa, H. M. J., Berg, L. K., Brito, J., Ching, J., Easter, R. C., Fan, J., Fast, J.
654   D., Feng, Z., Fuentes, J. D., Glasius, M., Goldstein, A. H., Alves, E. G., Gomes, H., Gu, D., Guenther, A., Jathar, S. H.,
655   Kim, S., Liu, Y., Lou, S., Martin, S. T., McNeill, V. F., Medeiros, A., de Sá, S. S., Shilling, J. E., Springston, S. R., Souza,
656   R. A. F., Thornton, J. A., Isaacman-VanWertz, G., Yee, L. D., Ynoue, R., Zaveri, R. A., Zelenyuk, A., and Zhao, C.:
657   Urban pollution greatly enhances formation of natural aerosols over the Amazon rainforest, Nat Commun, 10, 1046,
658   10.1038/s41467-019-08909-4, 2019.
659 Stolzenburg, D., Simon, M., Ranjithkumar, A., Kürten, A., Lehtipalo, K., Gordon, H., Ehrhart, S., Finkenzeller, H.,
660   Pichelstorfer, L., Nieminen, T., He, X.-C., Brilke, S., Xiao, M., Amorim, A., Baalbaki, R., Baccarini, A., Beck, L.,
661   Bräkling, S., Caudillo Murillo, L., Chen, D., Chu, B., Dada, L., Dias, A., Dommen, J., Duplissy, J., El Haddad, I., Fischer,
662   L., Gonzalez Carracedo, L., Heinritzi, M., Kim, C., Koenig, T. K., Kong, W., Lamkaddam, H., Lee, C. P., Leiminger, M.,
663   Li, Z., Makhmutov, V., Manninen, H. E., Marie, G., Marten, R., Müller, T., Nie, W., Partoll, E., Petäjä, T., Pfeifer, J.,
664   Philippov, M., Rissanen, M. P., Rörup, B., Schobesberger, S., Schuchmann, S., Shen, J., Sipilä, M., Steiner, G., Stozhkov,
665   Y., Tauber, C., Tham, Y. J., Tomé, A., Vazquez-Pufleau, M., Wagner, A. C., Wang, M., Wang, Y., Weber, S. K., Wimmer,
666   D., Wlasits, P. J., Wu, Y., Ye, Q., Zauner-Wieczorek, M., Baltensperger, U., Carslaw, K. S., Curtius, J., Donahue, N. M.,
667   Flagan, R. C., Hansel, A., Kulmala, M., Lelieveld, J., Volkamer, R., Kirkby, J., and Winkler, P. M.: Enhanced growth
668   rate of atmospheric particles from sulfuric acid, Atmos Chem Phys, 20, 7359-7372, 10.5194/acp-20-7359-2020, 2020.
669 Wang, L., Lal, V., Khalizov, A. F., and Zhang, R.: Heterogeneous Chemistry of Alkylamines with Sulfuric Acid: Implications
670   for Atmospheric Formation of Alkylaminium Sulfates, Environmental Science & Technology, 44, 2461-2465,
671   10.1021/es9036868, 2010.
672 Wang, Z.-Q., Liu, Y.-R., Wang, C.-Y., Jiang, S., Feng, Y.-J., Huang, T., and Huang, W.: Multicomponent nucleation of
673   malonic acid involved in the sulfuric acid - dimethylamine system and its atmospheric implications, Atmos Environ, 267,
674   118558, https://doi.org/10.1016/j.atmosenv.2021.118558, 2021.
675 Wu, Z. J., Hu, M., Liu, S., Wehner, B., Bauer, S., Ssling, A. M., Wiedensohler, A., Petaja, T., Dal Maso, M., and Kulmala,
676   M.: New particle formation in Beijing, China: Statistical analysis of a 1-year data set, J Geophys Res-Atmos, 112, 2007.
677 Xiao, S., Wang, M. Y., Yao, L., Kulmala, M., Zhou, B., Yang, X., Chen, J. M., Wang, D. F., Fu, Q. Y., Worsnop, D. R., and
678   Wang, L.: Strong atmospheric new particle formation in winter in urban Shanghai, China, Atmospheric Chemistry and
679   Physics, 15, 1769-1781, 10.5194/acp-15-1769-2015, 2015.
680 Yang, D., Zhu, S., Ma, Y., Zhou, L., Zheng, F., Wang, L., Jiang, J., and Zheng, J.: Emissions of Ammonia and Other Nitrogen-
681   Containing Volatile Organic Compounds from Motor Vehicles under Low-Speed Driving Conditions, Environmental
682   Science & Technology, 56, 5440-5447, 10.1021/acs.est.2c00555, 2022.
683 Yang, S., Liu, Z., Clusius, P. S., Liu, Y., Zou, J., Yang, Y., Zhao, S., Zhang, G., Xu, Z., Ma, Z., Yang, Y., Sun, J., Pan, Y., Ji,
684   D., Hu, B., Yan, C., Boy, M., Kulmala, M., and Wang, Y.: Chemistry of new particle formation and growth events during
685   wintertime in suburban area of Beijing: Insights from highly polluted atmosphere, Atmospheric Research, 255, 105553,
686   https://doi.org/10.1016/j.atmosres.2021.105553, 2021.
687 Yao, L., Garmash, O., Bianchi, F., Zheng, J., Yan, C., Kontkanen, J., Junninen, H., Mazon, S. B., Ehn, M., Paasonen, P., Sipila,
688   M., Wang, M. Y., Wang, X. K., Xiao, S., Chen, H. F., Lu, Y. Q., Zhang, B. W., Wang, D. F., Fu, Q. Y., Geng, F. H., Li,
689   L., Wang, H. L., Qiao, L. P., Yang, X., Chen, J. M., Kerminen, V. M., Petaja, T., Worsnop, D. R., Kulmala, M., and
690   Wang, L.: Atmospheric new particle formation from sulfuric acid and amines in a Chinese megacity, Science, 361, 278-
691   281, 2018.
692 Yin, R., Yan, C., Cai, R., Li, X., Shen, J., Lu, Y., Schobesberger, S., Fu, Y., Deng, C., Wang, L., Liu, Y., Zheng, J., Xie, H.,
693   Bianchi, F., Worsnop, D. R., Kulmala, M., and Jiang, J.: Acid–Base Clusters during Atmospheric New Particle Formation
694   in Urban Beijing, Environmental Science & Technology, 55, 10994-11005, 10.1021/acs.est.1c02701, 2021.
695 Yu, F.: From molecular clusters to nanoparticles: second-generation ion-mediated nucleation model, Atmos Chem Phys, 6,
696   5193-5211, 2006.
697 Yu, F. Q. and Turco, R. P.: From molecular clusters to nanoparticles: Role of ambient ionization in tropospheric aerosol
698   formation, J Geophys Res-Atmos, 106, 4797-4814, 2001.
699 Zaveri, R. A., Easter, R. C., Shilling, J. E., and Seinfeld, J. H.: Modeling kinetic partitioning of secondary organic aerosol and
700   size distribution dynamics: representing effects of volatility, phase state, and particle-phase reaction, Atmos Chem Phys,
701   14, 5153-5181, 2014.
702 Zhao, B., Shrivastava, M., Donahue, N. M., Gordon, H., Schervish, M., Shilling, J. E., Zaveri, R. A., Wang, J., Andreae, M.
703   O., Zhao, C., Gaudet, B., Liu, Y., Fan, J., and Fast, J. D.: High concentration of ultrafine particles in the Amazon free
704   troposphere produced by organic new particle formation, Proc Natl Acad Sci U S A, 117, 25344-25351,
705   10.1073/pnas.2006716117, 2020.
706 Zheng, H., Cai, S., Wang, S., Zhao, B., Chang, X., and Hao, J.: Development of a unit-based industrial emission inventory in
707   the Beijing–Tianjin–Hebei region and resulting improvement in air quality modeling, Atmospheric Chemistry and
708   Physics, 19, 3447-3462, 10.5194/acp-19-3447-2019, 2019.
709 Zheng, J., Ma, Y., Chen, M., Zhang, Q., Wang, L., Khalizov, A. F., Yao, L., Wang, Z., Wang, X., and Chen, L.: Measurement
710   of atmospheric amines and ammonia using the high resolution time-of-flight chemical ionization mass spectrometry,
711   Atmos Environ, 102, 249-259, 10.1016/j.atmosenv.2014.12.002, 2015a.
712 Zheng, J., Ma, Y., Chen, M. D., Zhang, Q., Wang, L., Khalizov, A. F., Yao, L., Wang, Z., Wang, X., and Chen, L. X.:
713   Measurement of atmospheric amines and ammonia using the high resolution time-of-flight chemical ionization mass
714   spectrometry, Atmos Environ, 102, 249-259, 2015b.

715 Zhu, S., Yan, C., Zheng, J., Chen, C., Ning, H., Yang, D., Wang, M., Ma, Y., Zhan, J., Hua, C., Yin, R., Li, Y., Liu, Y., Jiang,
716   J., Yao, L., Wang, L., Kulmala, M., and Worsnop, D. R.: Observation and Source Apportionment of Atmospheric Alkaline
717   Gases in Urban Beijing, Environmental Science & Technology, 56, 17545-17555, 10.1021/acs.est.2c03584, 2022.

718

719
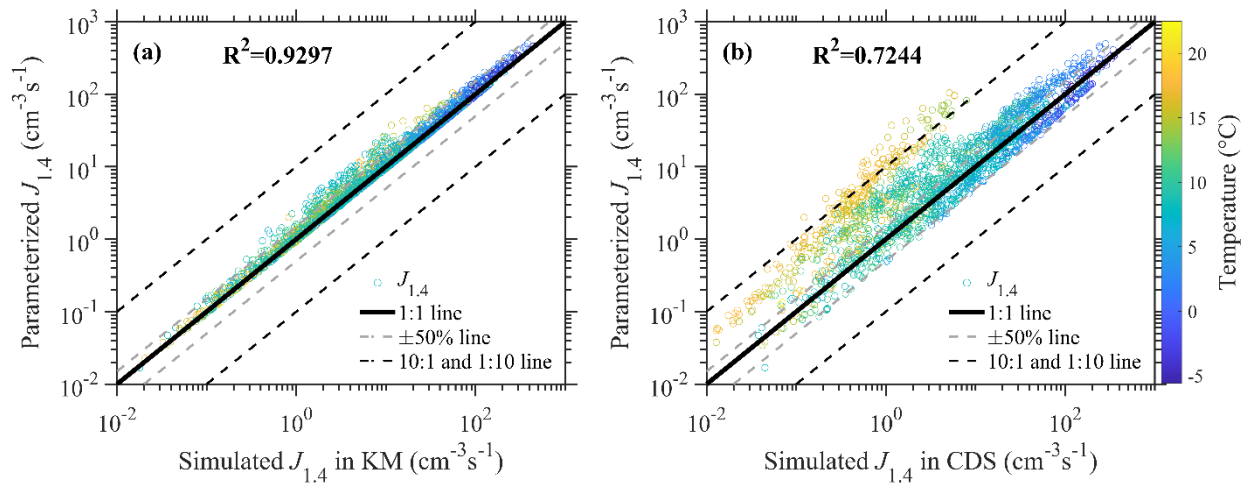
Figure 1. $J_{1.4}$ **Comparison of simplified parameterization method with kinetic model (KM) results (a) and cluster dynamic simulation (CDS) results (b).** The red hollow circles showed the simulation results according to atmospheric observation data. The grey straight line represents the 1:1 line, while the grey dashed line represents the ±50% variation and the black dashed lines represent 1:10 or 10:1 line. The circles are colored by the temperatures.

724
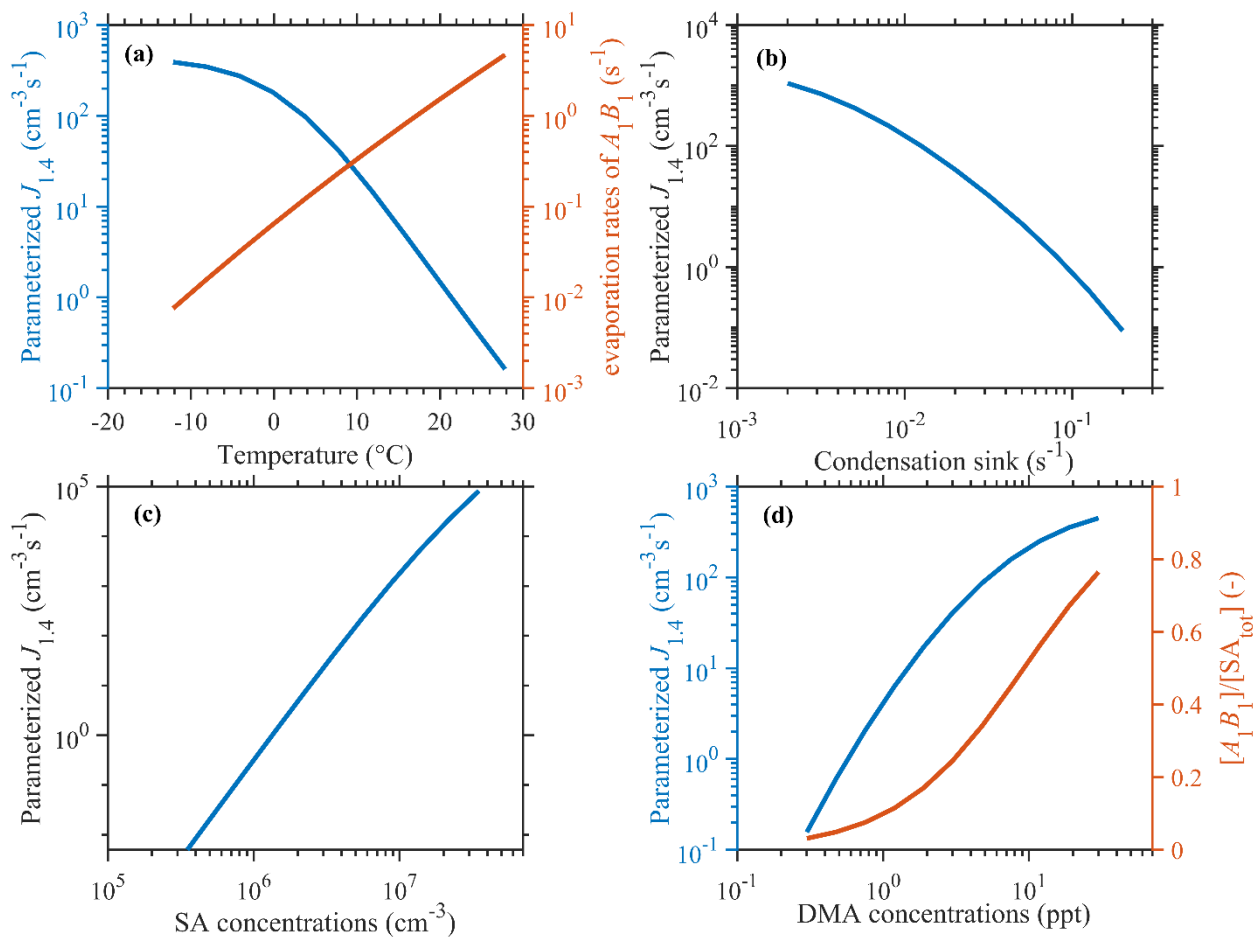
Figure 2. Dependence of simulation results on varying **T, CS, [DMA], [SA].** The values of fixed parameters are 281K, 0.02 s^{-1}, 3 ppt, and 3.5$\times 10^6$ cm^{-3}, respectively, as median values during NPF events in our simulation period.

727
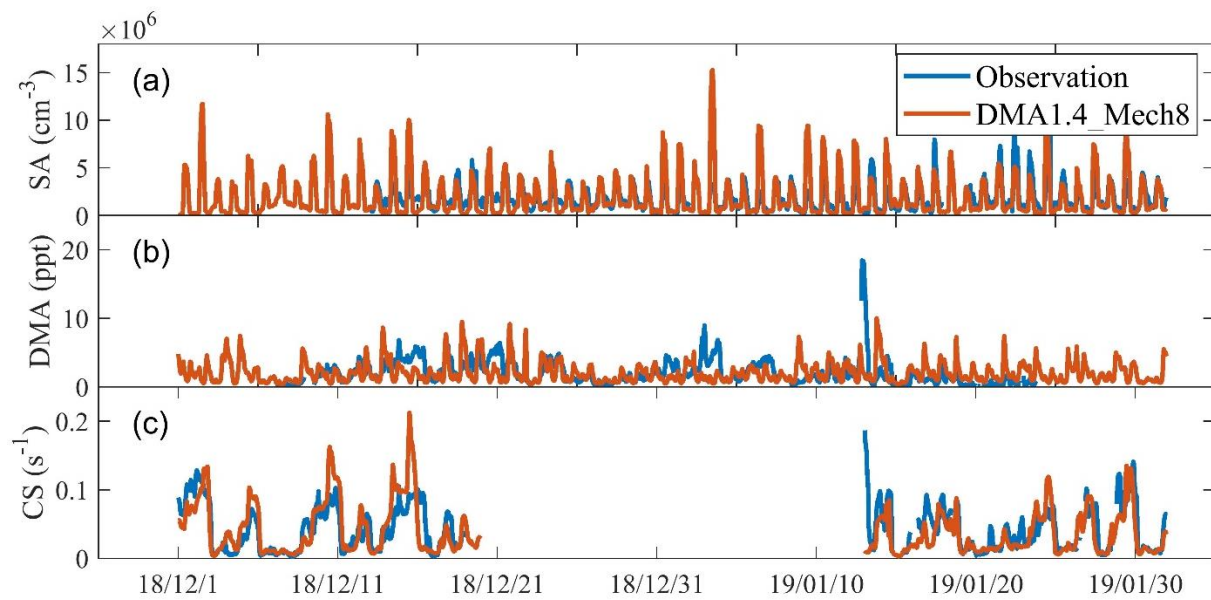
Figure 3. Comparison of simulated concentrations of DMA (a), SA (b). and CS during periods with full PNSD observation (c) with field measurements for wintertime Beijing (December 2018 and January 2019).

730
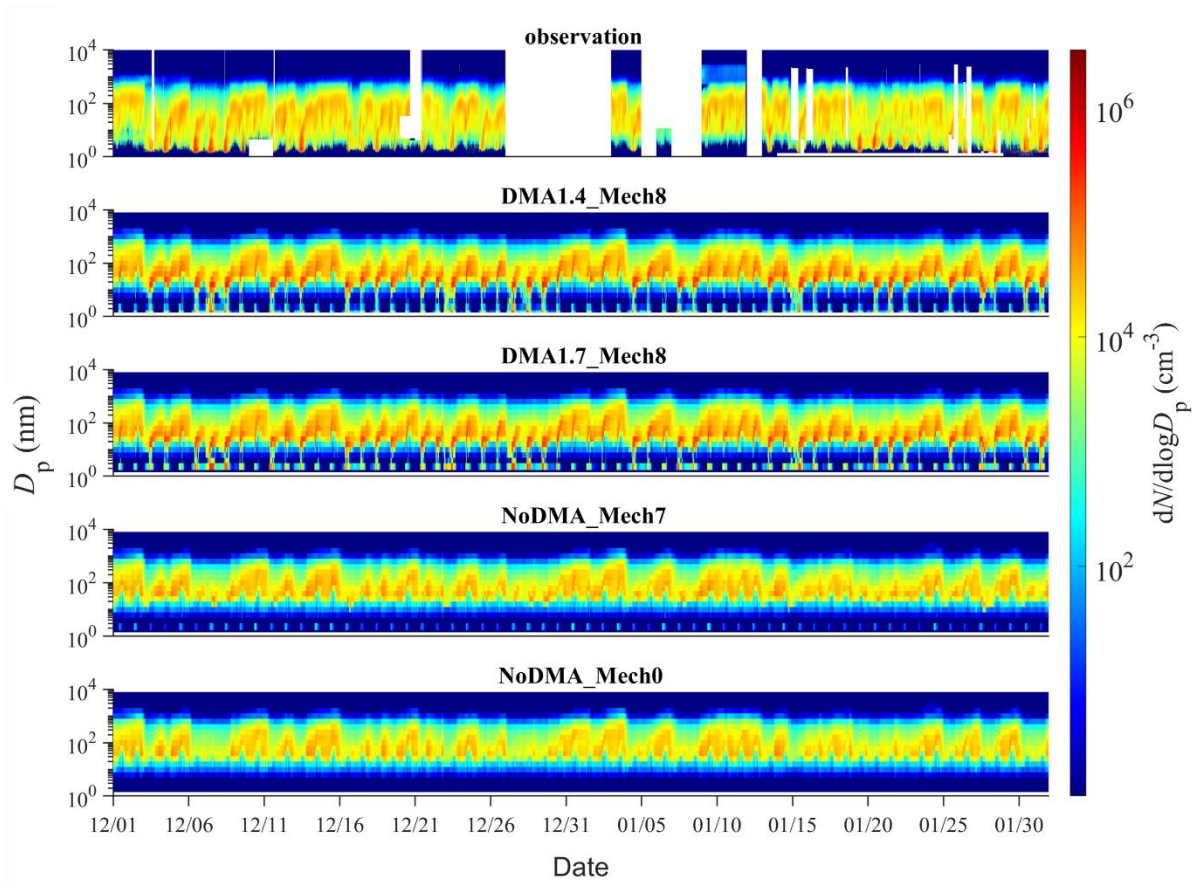
Figure 4. Comparison of time series of particle number size distribution simulated by various scenarios with the observed one. Description of four scenarios is detailed in ***Configuration of the Updated WRF-Chem/R2D-VBS Model*** section.

734
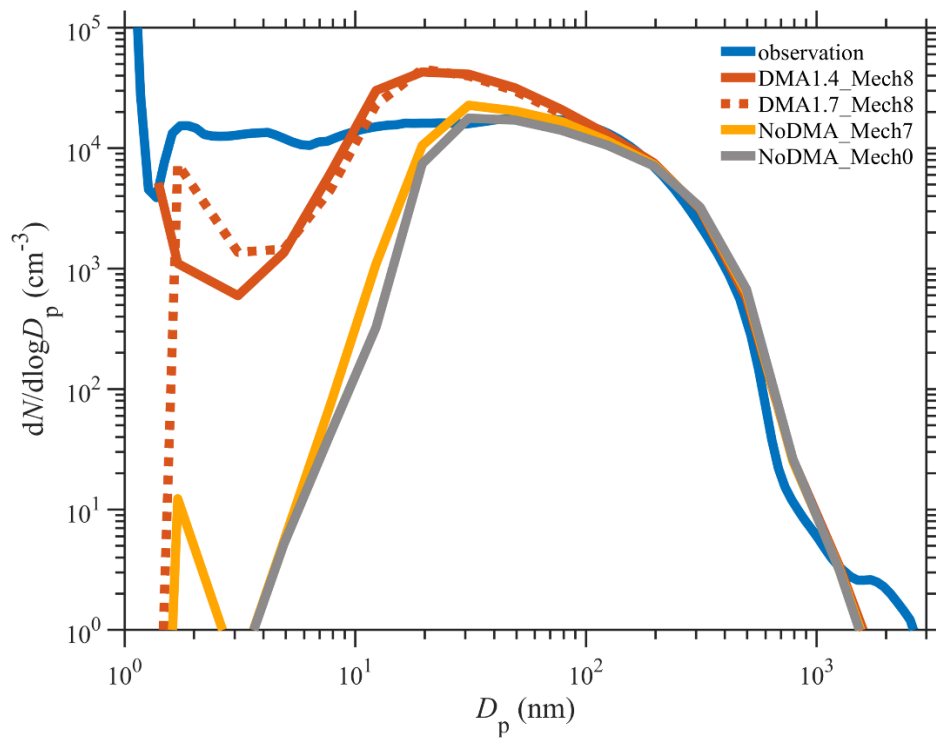
Figure 5. Comparison of averaged particle number size distribution simulated by various scenarios with the observed one. Description of four scenarios is detailed in *Configuration of the Updated WRF-Chem/R2D-VBS Model* section.

737
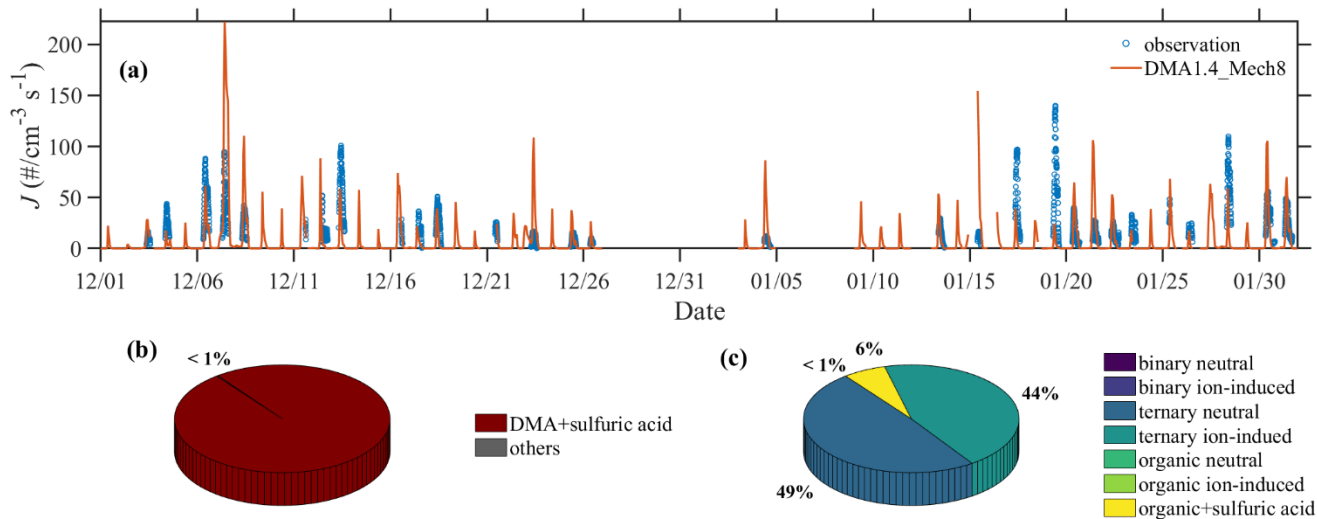
Figure 6. Comparison of simulated nucleation rates with those derived from field measurements (a), and contribution from different nucleation mechanisms (b) with a special illustration of nucleation pathways other than SA-DMA (c).